Depth profiles of vacancy- and interstitial-type defects in MeV implanted Si

S. Coffa[a] and V. Privitera
CNR-IMETEM, Stradale Primosole 50, I95121 Catania, Italy

F. Priolo, S. Libertino, and G. Mannino
INFM and Dipartimento di Fisica, Corso Italia 57, I95129 Catania, Italy

(Received 7 August 1996; accepted for publication 6 November 1996)

We demonstrate that the depth distribution of defects in MeV implanted n-type and p-type crystalline Si is severely affected by the impurity content of the material. Silicon samples with different concentrations of dopants (P or B) and intrinsic contaminants (i.e., C and O) were implanted with 1 or 2 MeV He ions to fluences in the range 2.5×10^{8}–1×10^{13}/cm^2. Using deep-level transient spectroscopy and spreading resistance measurements, we have identified the defects and determined their concentration and depth distribution. It is found that less than 4% of the defects generated by the beam escape recombination and are stored in electrically active, room temperature stable defect clusters, such as divacancies and carbon–oxygen pairs. When the concentration of these defects is much smaller than the doping level, their profile mirrors the initial defect distribution, as calculated by transport of ions in matter (TRIM), a Monte Carlo code. In particular, the profile presents a maximum at the same depth predicted by TRIM and a width which is strongly dependent on the impurity content of the substrate. Indeed this width can be as large as 2 μm when implants are performed on a lightly doped, pure epitaxial substrate and returns to the value predicted by TRIM ($\sim$0.5 μm) upon increasing the concentration of dopants and intrinsic contaminants which act as traps for the diffusing point defects. The broadening of the concentration profiles is however shown to be unavoidable at high implantation fluences when most of the traps are already full and unable to interrupt the free migration of newly generated defects. Finally, by comparing defect distributions in n-type and p-type samples we have detected the spatial separation between vacancy-type and interstitial-type defects, resulting from the ion momentum transfer. The observed phenomena are explained in terms of a trap limited diffusion of the defects generated by the beam. These effects are only observable for a light ion such as He since direct defect clustering within the diluted collision cascades is expected to be significantly inhibited. © *1997 American Institute of Physics.* [S0021-8979(97)02604-2]

I. INTRODUCTION

The room temperature (RT) migration and clustering properties of ion beam generated defects in crystalline silicon has been the target of several recent experimental[1–5] and theoretical[6,7] investigations. This interest is driven by the fact that these properties determine the dynamic evolution of damage during ion implantation and the final defect structure in ion-implanted silicon. In spite of the fact that various studies focused on the defect properties of ion implanted material, several issues are still unclear. For example, the role of the impurity content of the substrate on the process of damage accumulation and on the defect depth distribution has not yet been clarified. Furthermore, since most of the recent investigations have used deep level transient spectroscopy (DLTS) measurements of as-implanted samples, they are limited to low fluence implants, for which the concentration of defects is much smaller than the dopant concentration. This is a quite serious limitation since it does not allow one to obtain information on the defect evolution at higher fluences. This information is of great technological interest since for these implants the post-annealing process is more critical and produces the well known effects of extended defect formation[8] and transient enhanced diffusion.[9,10]

Most recently we have shown[2,3] that the room temperature migration properties of ion beam generated defects strongly depend on the impurity content of the material. In fact, the defects undergo fast migration until they are trapped at dopant atoms or impurities present in the substrate. This effect is expected to play a major role in determining the defect depth distribution in MeV implanted Si. This is particularly true for a light mass ion since, because the collision cascade diluted quite a bit, some of the point defects [i.e., vacancies (V) and self-interstitials (I)] generated by the beam can escape recombination and direct clustering. Therefore, the migration and agglomeration properties of these defects can be explored. In this paper we use DLTS and spreading resistance profiling (SRP) measurements to monitor the defect distributions produced by MeV He implants over a wide range of fluences (both below and above that required to achieve significant compensation of the dopant) and for different dopant and impurity contents in the substrate. This allowed us to obtain a precise description of the defect-defect and defect-impurity interactions which determine damage evolution in ion implanted crystalline Si.

II. EXPERIMENTAL

In this work we used (100) oriented n-type (P-doped) and p-type (B-doped) crystalline Si wafers. In particular, epi-

[a]Electronic mail: coffa@ct.infn.it

taxially grown Si layers (Epi) and Czochralski (CZ) grown wafers have been used with resistivities in the range 10^{-2}–10^{2} Ω cm. This allowed us to analyze samples with widely different concentrations of the dopant (P or B, varied in the range 5×10^{13}–3×10^{18}/cm^3) and of the intrinsic contaminants (i.e., C and O, varied in the range $\sim10^{15}$ –10^{18}/cm^3). These samples were implanted at room temperature with He ions at energies of 1 or 2 MeV and to fluences in the range 2.5×10^{8}–1×10^{13}/cm^2. The resistivity changes produced by these implants were measured by SRP measurements. The spreading resistance values were converted into resistivity values using a set of calibrated samples. Furthermore the resistivity was converted into defect concentration by solving the charge neutrality equation, taking into account the concentration of charged defects, with a procedure described elsewhere.[11]

The same implants were also performed on p^+-n (or n^+-p) diodes realized by B (or P) diffusion in the n-type (p-type) Si substrate, giving a junction at a depth of ~0.3 μm. DLTS measurements were performed by reverse biasing the diode at a voltage suitable to include all of the damage region within the depletion layer and using a filling pulse at 0.3 V with a duration of 1 ms. Defect concentration profiles were obtained[12] by measuring the DLTS spectra at a constant reverse bias and changing the voltage of the filling pulse, in order to explore regions at different depths.

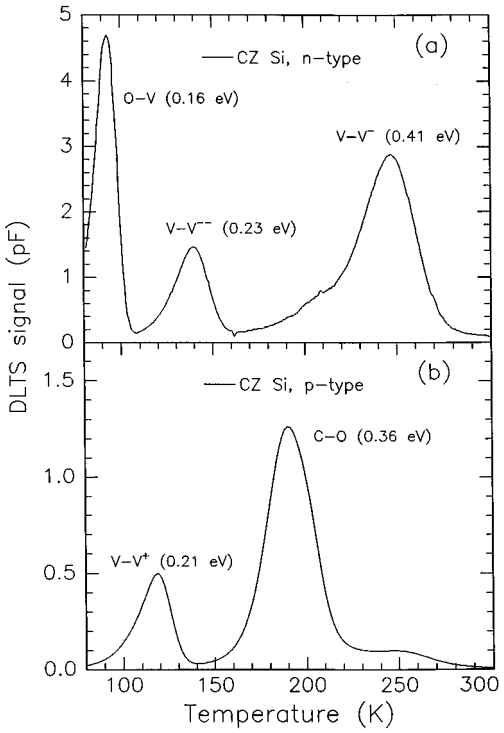

FIG. 1. DLTS spectra of a Czochralski, n-type (2 Ω×cm, P-doped) silicon sample (a) and of a Czochralski p-type (4 Ω×cm, B-doped) Si sample (b) implanted at 300 K with 1 MeV He to a fluence of 1×10^{10}/cm^2.

III. RESULTS AND DISCUSSIONS

A. Low fluence implants: Effect of the impurity content on defect concentration profiles

Ion implantation of MeV He ions in crystalline Si results in the formation of electrically active defect clusters which we have monitored using both DLTS and SRP measurements. A DLTS spectrum measured in a n-type CZ sample (2 Ω cm) implanted with 1×10^{10}/cm^2 He at 1 MeV is reported in Fig. 1(a). The signature of vacancy-type defect clusters is clearly visible. In fact, three levels are found at $E_c-0.41$ eV (single charged divacancy), $E_c-0.23$ eV (double charged divacancy), and $E_c-0.16$ eV (oxygen vacancy complex). A contribution due to the phosphorus-vacancy complex is also present under the dominating peak at $E_c-0.41$ eV. Its contribution has been estimated to be ~20%. In Fig. 1(b) we report the DLTS spectrum measured on a p-type CZ sample (4 Ω cm) implanted under the same conditions (1 MeV He to a fluence of 1×10^{10}/cm^2). Two different levels at $E_v+0.36$ eV and $E_v+0.21$ eV are observed due to carbon–oxygen complexes and to the single positively charged divacancies, respectively. The defect structures revealed by the measurements of Figs. 1(a) and 1(b) arise from the clustering of the point defects (V and I) generated by the ion beam. It is interesting to note that while the deep level spectrum of the n-type sample is dominated by vacancy-type defect clusters, an interstitial-type defect cluster (i.e., the carbon–oxygen complex) dominates the spectrum of the p-type samples.

The deep levels introduced by the defect complexes act as traps for the majority carriers and hence, when present at sufficiently high concentrations, they are able to produce a large increase in the resistivity of the sample. The defects can therefore also be detected by resistivity measurements. The resistivity profile, measured by SRP on a CZ n-type sample implanted with 2 MeV He at a fluence of 1×10^{11}/cm^2, is reported in Fig. 2(a). The resistivity of the unperturbed substrate (2 Ω cm) is strongly modified by this implantation in particular the resistivity increases as a function of depth, reaches a maximum of ~100 Ω cm at a depth of 6.2 μm, and then returns to the value of the unperturbed substrate.

The resistivity profile of Fig. 2(a) can be converted into a defect concentration profile by solving the neutrality charge equation, given by

$$p+N_P^+=n+N_{VV}^-+2N_{VV}^{--}, \tag{1}$$

where p and n are the concentrations of free holes and electrons respectively; N_P^+ is the concentration of dopants in the substrate; N_{VV}^- and N_{VV}^{--} are the concentrations of single charged and double charged divacancies given by

$$N_{VV}^-=\frac{N_{VV}^{\mathrm{tot}}}{1+X_{VV^-}\exp\left(\dfrac{E_{VV^-}-E_F}{kT}\right)},$$

$$N_{VV}^{--}=\frac{N_{VV}^{\mathrm{tot}}}{1+X_{VV^{--}}\exp\left(\dfrac{E_{VV^{--}}-E_F}{kT}\right)},$$

where V_{VV}^{tot} is the total divacancy concentration, E_F is the Fermi level position in the sample, X_{VV^-} and $X_{VV^{--}}$ are the entropy factors for the ionization of the two divacancy energy levels at $E_c-0.41$ eV and $E_c-0.23$ eV, respectively.

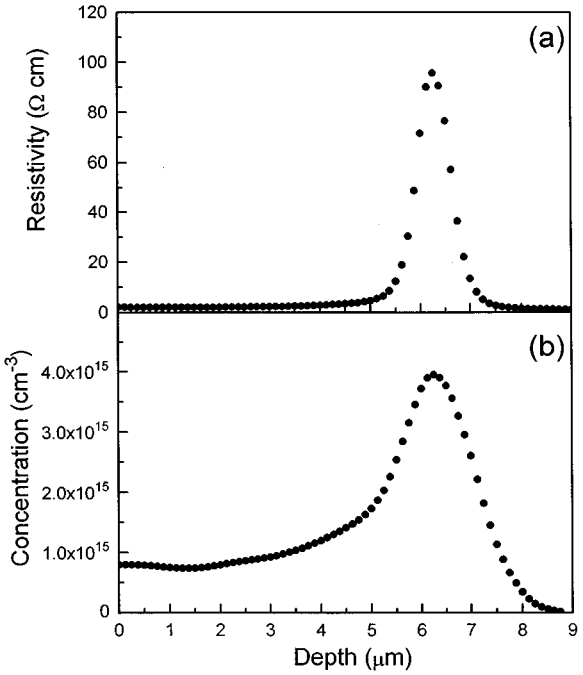

FIG. 2. (a) Resistivity profile as obtained by SRP measurements on a Czochralski sample (2 Ω×cm, *P*-doped) implanted at 300 K with 2 MeV He ions to a fluence of 1×10^{11}/cm^2; (b) defect concentration profiles obtained by the resistivity profile reported in (a) and by solving the neutrality charge equation.

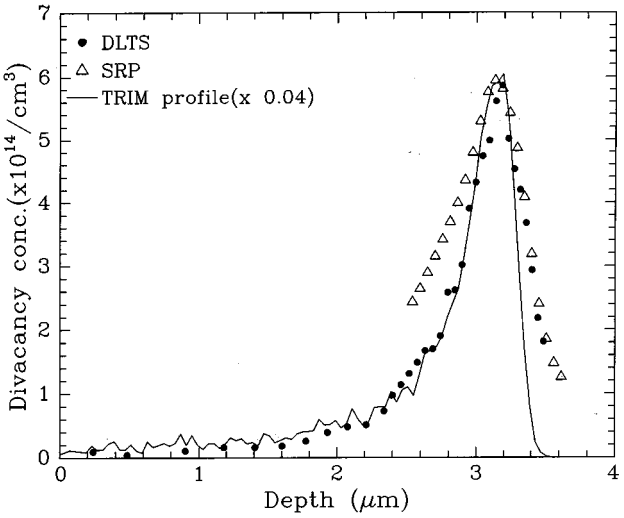

FIG. 3. Defect concentration profiles for a Czochralski Si sample implanted with 1 MeV He ions to a fluence of 1×10^{10}/cm^2. The defect profiles were measured on the same sample by DLTS (●) or by SRP measurements (△).

Equation (1) was solved using literature values[13] for the two entropy factors. In solving the neutrality charge equation (1), we have neglected the small contribution due to the P-V complexes. The contribution of the oxygen vacancy level was also neglected since, being so shallow, it is not occupied at room temperature and hence unable to produce compensation (note that the Fermi level before irradiation is at $E_c-0.26$ eV). The resulting defect concentration profile (N_{VV}^{tot}) is reported in Fig. 2(b). The large concentration of defects, being higher than the concentration of dopants (1×10^{15}/cm^3), produces a large compensation and hence the resistivity enhancement reported in Fig. 2(a).

It should be noted that the conditions for a successful application of DLTS and SRP measurements are quite different. In fact concentration profiles can be derived from DLTS analyses only if the trap concentration is lower that the dopant concentration. On the other hand dopant compensation is required for defect concentration evaluation from SRP measurements, since a resistivity increase can be detected only when the concentration of defects is comparable to the concentration of dopants. Therefore it is quite difficult to perform meaningful measurements with both techniques on the same sample. However, since a significant variation in resistivity can be also obtained when the defect concentration is only ~20% of the dopant concentration, by tuning the ion fluence we were able to prepare a sample in which a direct comparison was possible. Indeed in Fig. 3 we show the concentration profiles of divacancies obtained by DLTS (●) and SRP (△) on a CZ sample implanted with 1 MeV He ions to a fluence of 1×10^{10}/cm^2. The agreement between the two determinations of the concentration profile is noteworthy and clearly indicates that SRP, although being a nonspectroscopic technique, can be used to profile defect concentration. In this application the excellent depth resolution (~10 nm, independent of the dopant concentration) and sensitivity of this technique can be of great help.

In Fig. 3 we also report as a solid line the initial defect distribution produced by the ion, as calculated by transport of ions in matter (TRIM).[14] In order to allow the comparison, this curve was divided by a factor of 25. From the comparison it emerges that only 8% of the point defects produced by the beam is stored in electrically active, room temperature stable defects (note that each defect contains two vacancies). This suggests that extensive recombination of the *V* and *I* produced by the beam (~92) occurs. Since each ion produces ~120 Frenkel pairs, this implies that only ~4 divacancies per ion are left. Moreover it is noteworthy to observe that, in spite of the extensive recombination, the defect distribution quite precisely mirrors the initial defect concentration, suggesting that long range migration of the defects does not occur in this material. However, we have found that the defect profiles in the low fluence regime are extremely sensitive to the impurity content of the substrate. In Fig. 4 we compare the concentration profiles of the divacancy level at $E_c-0.41$ eV, measured by DLTS, on *n*-type samples having different dopant and impurity contents and implanted with 1 MeV He to a fluence of 5×10^8/cm^2. The data of Fig. 4 allow one to explore the efficiency of P and O as traps for migrating vacancies. The role of oxygen can be understood by comparing the divacancy concentration profile in an epitaxial wafer (○), having a low oxygen content ($<10^{16}$ O/cm^3), and in a Czochralski wafer (●), which has a high oxygen content ($\sim10^{18}$ O/cm^3) both doped with a similar P concentration (2×10^{15} P/cm^3 for the CZ sample and 7×10^{14}/cm^3 for the epitaxial sample). In the CZ sample the divacancy concentration profile mirrors quite precisely the initial defect generation profile, calculated by TRIM, which is reported as a solid line in Fig. 4. For the epitaxial layer the defect distri-

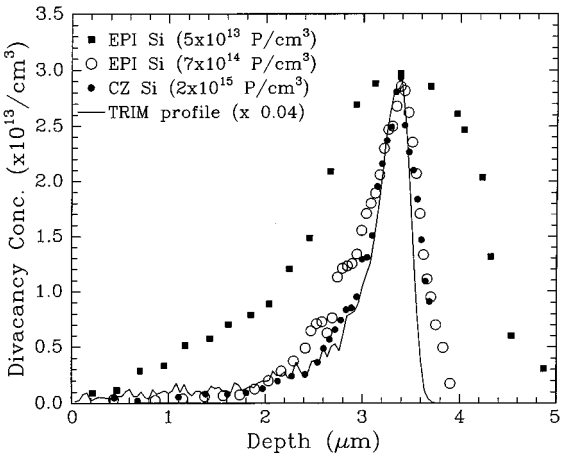

FIG. 4. Divacancy concentration profiles obtained by DLTS measurements on a Czochralski Si sample doped with 2×10^{15} P/cm^3 (●), on an epitaxial Si layer doped with 7×10^{14}/cm^3 (○) and on an epitaxial Si layer doped with 5×10^{13} P/cm^3 (■). The samples were implanted at room temperature with 1 MeV He to a fluence of 5×10^8/cm^2.

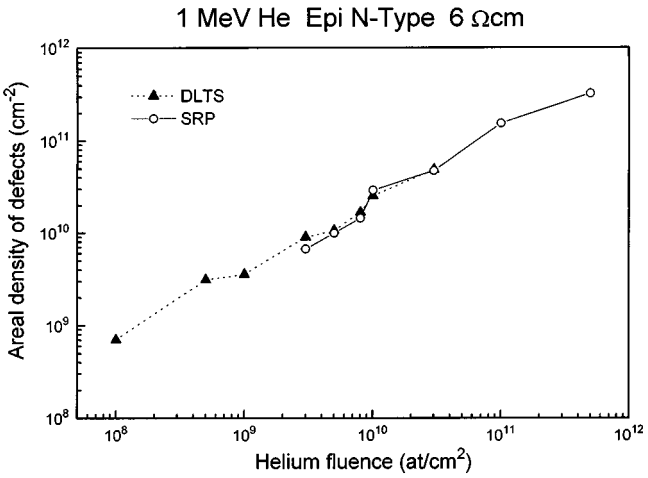

FIG. 5. Areal density of defects as a function of ion fluence for 1 MeV He implants on n-type epitaxial Si layer, with a P content of 7×10^{14}/cm^3. The data were obtained by DLTS (△) and SRP (○).

bution is instead slightly broader suggesting that the defects are able to undergo a short migration before clustering with impurities or other defects. This is expected since O is known to act as a trap for vacancies through the formation of oxygen–vacancy complexes. The data of Fig. 4 also demonstrate that P is a very efficient trap for the vacancies. In fact the divacancy concentration profile measured in a lowly n-type doped (5×10^{13}/cm^3, ■) epitaxial layer has a much broader width (~2 μm) than that (~0.6 μm) measured for the divacancy profile in the epitaxial layer with higher P content (7×10^{14}/cm^3, ○). This result implies that P is very efficient in trapping the vacancies since increasing the P concentration from 5×10^{13}/cm^3 to 7×10^{14}/cm^3 results in an almost complete suppression of vacancy migration. This effect is probably due to the formation of phosphorus–vacancy complexes which immobilize the vacancies.

B. High fluence implants: The evolution of the defect profiles

The defect distributions in samples implanted at high He fluences, when extensive dopant compensation occurs, have been measured by SRP. In Fig. 5 we report the areal density of defects (obtained by integrating the defect concentration profiles) as a function of He fluences. These values were determined by DLTS at low fluences (triangles) and by SRP at higher fluences (open circles). The good match between the two sets of data once more confirms the good agreement between the two techniques. It is interesting to note that the increase of defect concentration with ion fluence is slightly sublinear: note for example that ~8 defects/ion are introduced at low fluences while only ~1.6 defects/ion are introduced at a fluence of 1×10^{11}/cm^2 and even lower values are obtained at higher fluences.

We have found that P, which severely affects the defect distribution in the low fluence regime (as we have shown in Sec. III A), also produces huge effects in the defect concentration profiles at high fluences. Some examples of these profiles, measured by SRP, are reported in Figs. 6(a) to (c). In Fig. 6(a) we report two profiles measured on a lightly n-type doped (5×10^{13} P/cm^3) epitaxial layer implanted with 2 MeV He at fluences of 1×10^9/cm^2 (△) and 5×10^{10}/cm^2 (□). It should be noted that the increase in the He fluence produces dramatic modifications in the shape of the defect profile. Particularly the profile broadens and the peak position shifts

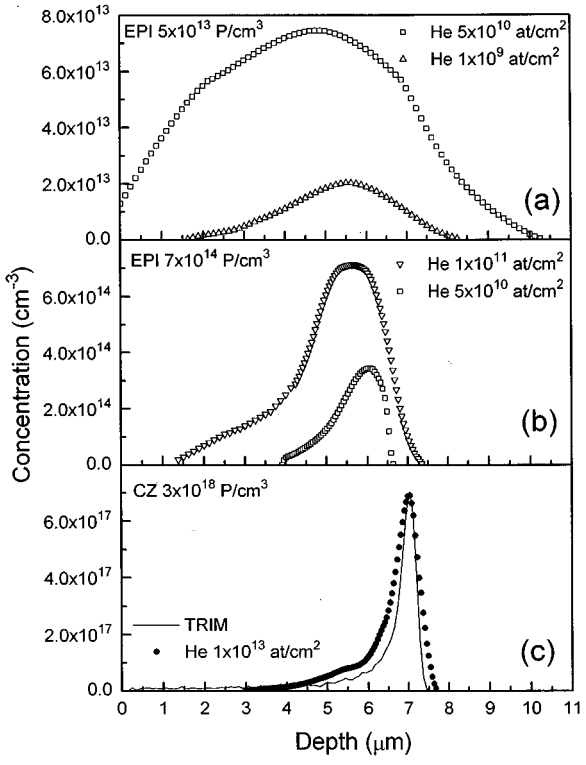

FIG. 6. Defect concentration profile, derived form SRP measurements, measured on n-type Si samples implanted with 2 MeV He: (a) 1×10^9/cm^2 (△) and 5×10^{10}/cm^2 (□) on an epitaxial layer with a P concentration of 5×10^{13}/cm^2; (b) 5×10^{10}/cm^2 (□) and 1×10^{11}/cm^2 (▽) on an epitaxial layer with a P concentration of 7×10^{14}/cm^2; (c) 1×10^{13}/cm^2 (●) on a CZ sample with a P concentration of 3×10^{18}/cm^3.

toward the surface. A similar behavior is also observed [Fig. 6(b)] for 2 MeV He implants at fluences of $5\times10^{10}/cm^2$ and $1\times10^{11}/cm^2$ in a *n*-type doped (7×10^{14} P/cm^3) epitaxial Si sample. Note however that, as a consequence of the increase in the P content, in this case the broadening of the profile is smaller and occurs at higher fluences. The strong effect of P is also confirmed by the fact that, when He implants are performed on a sample with a very high P concentration ($3\times10^{18}/cm^3$), the measured defect profile mirrors the TRIM profile (solid line) even for a rather high ($1\times10^{13}/cm^2$) He fluence [Fig. 6(c)]. The results of Fig. 6 confirm once more that P is a very efficient trap for vacancies. The observed broadening of the defect concentration profile [Figs. 6(a) and (b)] can be explained by assuming that the free migration of the vacancies produced by the beam is interrupted by trapping at the P atoms. When the He fluence is increased, a condition is reached in which most of the P atoms are embodied into defect complexes and are therefore unable to act as effective traps for the new defect generated by the beam. This also explains while broadening of the profile will not occur (even at very high He fluences) in samples with a very high P content [Fig. 6(c)].

A striking characteristic of the profiles reported in Fig. 6 is the fact that the defect profiles preferentially broaden toward the surface. This can be tentatively explained assuming that V motion towards the bulk is impeded by the high density of interstitial-type defects which, due to the momentum transferred by the ion, are located deeper than the vacancy-type defects. An alternative explanation is that vacancies undergo radiation enhanced diffusion in the region directly modified by the beam and are hence only able to migrate toward the surface.

In Fig. 7 we summarize the measured values of the peak position [Fig. 7(a)] and width [Fig. 7(b)] of the defect distribution as a function of the He fluence for two epitaxial layers with P-doping of $5\times10^{13}/cm^3$ (triangles) and $7\times10^{14}/cm^3$ (circles), and on a CZ Si sample doped with P at a concentration of $3\times10^{18}/cm^3$ (squares) are reported. Data at low fluences (open symbols) were derived from DLTS defect profiles, while at higher fluences the peak position and the width of the profiles were measured by SRP (closed symbols). Once more it is evident that large variations in the peak position and width of the profiles, with respect to those calculated by TRIM (reported as solid lines in Fig. 7), occur when the He fluence is increased. As a matter of fact, the He fluences at which significant variation occurs shift to higher values upon increasing the P content of the material.

C. Interstitial and vacancy-type defects: Comparison of He implants in *n*- and *p*-type Si

The DLTS analyses of Fig. 1 demonstrate that the deep level spectrum is dominated by the signature of interstitial-type defects in *p*-type and of vacancy-type defects in *n*-type samples. These defect complexes also dominate majority carrier processes and hence resistivity increases in the material. In order to have information on the spatial location of interstitial and vacancy-type defects, it is therefore interesting to compare the resistivity profiles measured in *p*- and *n*-type silicon.

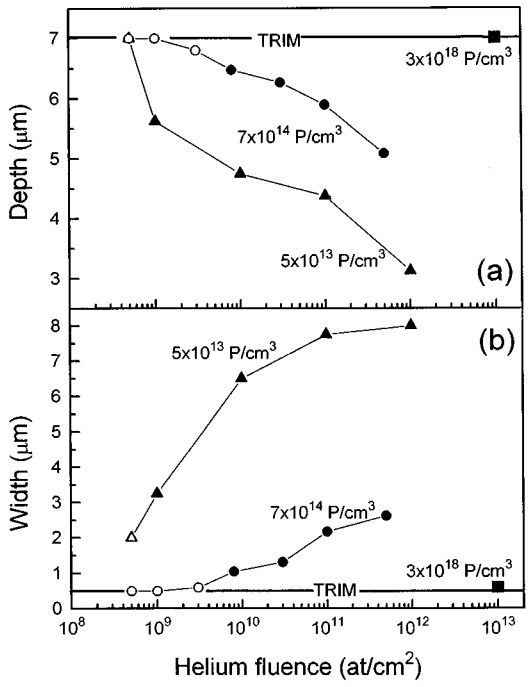

FIG. 7. Variation of the width and peak position of the defect profile as a function of He fluence for three different *n*-type Si sample: (1) an epitaxial Si layer with a *P* content of $5\times10^{13}/cm^3$ (triangles); (2) an epitaxial Si layer with a *P* content of $7\times10^{14}/cm^3$ (circles); (3) a CZ Si sample with a *P* content of $3\times10^{18}/cm^3$, (squares). Measurements were obtained by DLTS (open symbols) and SRP (closed symbols).

For *p*-type samples we have performed a study similar to the one presented in the previous section for *n*-type samples. We have found that the evolution of the defect profiles as a function of the He fluence and impurity concentration is very similar to that observed for *n*-type silicon. Once again, at low fluence (when the defect concentration is much smaller than the dopant concentration) the defect profiles present a maximum at a depth coinciding with that predicted by TRIM, while the width of the defect distribution is very sensitive to the impurity content of the substrate. Furthermore, a large broadening of the profile is observed in highly pure materials when most of the traps for the defects are saturated.

New and interesting features emerge, however, when the resistivity profiles obtained in *n*- and *p*-type silicon are compared for the same He implant (Fig. 8). Each profile in Fig. 8 is normalized to its maximum value. Two extreme cases are considered: (1) low fluence implant ($1\times10^{11}/cm^2$, 2 MeV He) into lightly doped ($\sim5\times10^{13}/cm^3$) *p*-type and *n*-type epitaxial layers [Fig. 8(a)]; (2) high He fluence ($1\times10^{13}/cm^2$, 2 MeV) into heavily doped ($3\times10^{18}/cm^3$) *n*- and *p*-type CZ substrates. In both cases it is evident that a clear depth separation exists between the deeper resistivity profile measured in *p*-type and the shallower resistivity profile measured in *n*-type silicon. This separation is quite small in the case of the heavily doped substrate and becomes much larger in the lightly doped epitaxial substrates. Since the resistivity profile of *n*-type samples is dominated by vacancy-type defects, while interstitial-type defects dominate the resistivity profile of *p*-type samples, the data of Fig. 8 imply that a spatial separation exists between vacancy and interstitial-type de-

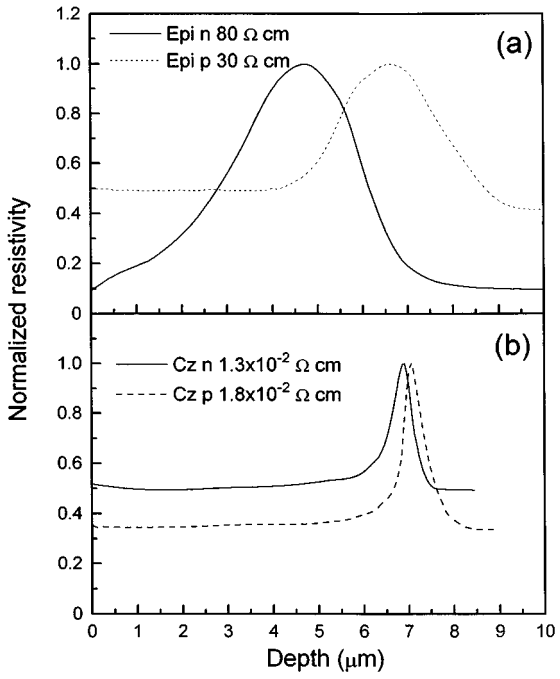

FIG. 8. (a) Comparison of the resistivity profiles obtained on lightly doped p-type and n-type epitaxial Si layers implanted with 2 MeV He to a fluence of $1\times10^{11}/\text{cm}^2$; (b) comparison of the resistivity profiles obtained on heavely doped p-type and n-type CZ Si samples implanted with 2 MeV He to a fluence of $1\times10^{13}/\text{cm}^2$.

fects generated by the beam. It is interesting to observe that this separation is expected on the basis of the momentum transferred by the ion which produces a deeper distribution of self-interstitials compared to vacancies. This effect is normally very small, difficult to detect, and expected to be visible only when extensive recombination of the ion generated defects occurs. This is indeed true in our case, since we have shown in Sec. III B that extensive recombination of the defects generated by MeV He ions occurs. The larger spatial separation observed in the lightly doped substrates can be explained by noting that the destiny of the defects that escape this direct recombination is determined by their nature and by their interaction with dopants, impurities, and other defects [2,3]. In the heavily doped substrate these defects will be immediately trapped by the formation of immobile complexes with dopants. On the other hand, in highly pure samples [like those of Fig. 8(a)], the low concentration of traps permits long range migration for the defects that escape recombination. In this case, vacancy type defects will exhibit preferential broadening toward the surface because interstitial type defects will impede their motion towards the bulk. In a similar fashion the vacancy-type defects will impede migration of interstitials toward the surface. These two effects will finally produce the large separation between vacancy-type and interstitial type defects which we have observed.

IV. CONCLUSIONS

We have shown that the defect concentration profiles in MeV He implanted Si are strongly dependent on the impurity content of the substrate. The use of a low mass ion such as He allows for the avoidance of direct clustering within the cascades and for observation of the migration of the defects generated by the beam. In fact, in spite of the fact that most of the Frenkel pairs (~96%) generated by the beam recombine, the destiny of the defects which escape recombination is strongly dependent on their nature and interaction with dopants, impurities, and other defects. By comparing the defect concentration profiles produced by MeV He implants into n-type and p-type samples, we have measured the spatial separation between interstitial- and vacancy-type defects arising from the momentum transfer of the ion.

ACKNOWLEDGMENTS

We would like to acknowledge S. U. Campisano and E. Rimini for several useful discussions. We would also like to thank A. Spada, N. Parasole, and A. Marino for expert technical assistance.

[1] B. G. Svennson, C. Jagadish, A. Hallén, and J. Lalita, Nucl. Instrum. Methods Phys. Res. B **106**, 183 (1995).
[2] K. Kyllesbech Larsen, V. Privitera, S. Coffa, F. Priolo, S. U. Campisano, and A. Carnera, Phys. Rev. Lett. **76**, 1493 (1996).
[3] V. Privitera, S. Coffa, F. Priolo, K. Kyllesbech Larsen, and G. Mannino, Appl. Phys. Lett. **68**, 3422 (1996).
[4] B. G. Svensson, C. Jagadish, and J. S. Williams, Phys. Rev. Lett. **71**, 1860 (1993).
[5] C. Christensen, J. W. Petersen, and A. Nylandsted Larsen, Appl. Phys. Lett. **61**, 1426 (1992).
[6] G. H. Gilmer, T. Diaz de la Rubia, D. M. Stock, and M. Jaraiz, Nucl. Instrum. Methods Phys. Res. B **102**, 247 (1995).
[7] M. Jaraiz, G. H. Gilmer, J. M. Poate, and T. D. de la Rubia, Appl. Phys. Lett. **68**, 409 (1996).
[8] K. S. Jones, S. Prussin, and E. R. Weber, Appl. Phys. A **45**, 1 (1988).
[9] P. A. Stolk, D. J. Eaglesham, H. J. Gossmann, and J. M. Poate, Appl. Phys. Lett. **66**, 1370 (1995).
[10] N. E. B. Cowern, K. T. F. Janssen, and H. F. F. Jos, J. Appl. Phys. **68**, 6191 (1990).
[11] A. Battaglia, S. Coffa, and F. Priolo, Appl. Phys. Lett. **65**, 306 (1994).
[12] D. V. Lang, J. Appl. Phys. **45**, 3023 (1974).
[13] S. D. Brotherton and P. Bradley, J. Appl. Phys. **53**, 5720 (1982).
[14] J. P. Biersack and L. G. Haggmark, Nucl. Instrum. Methods **174**, 257 (1980).